This article has been accepted for publication in a future issue of this journal, but has not been fully edited. Content may change prior to final publication. Citation information: DOI 10.1109/TNB.2018.2826919, IEEE Transactions on NanoBioscience

On the Response of Nanoelectrode Impedance Spectroscopy Measures to Plant, Animal, and Human Viruses

Andrea Cossettini[1], *Student Member, IEEE*, and Luca Selmi[1,2], *Fellow, IEEE*

***Abstract*—A simplified lumped geometrical and electrical model for the high frequency impedance spectroscopy (HFIS) response of nanoelectrodes to T=3 capsids and full viruses is developed starting from atomistic descriptions, in order to test the theoretical response of a realistic HFIS CMOS biosensor platform to different viruses. Capacitance spectra are computed for plant (CCMV), animal (RHDV), and human (HAV) viruses. A few common features of the spectra are highlighted and the role of virus charge, pH, and ionic strength on the expected signal is discussed. They suggest that the frequency of highest sensitivity at nearly physiological concentrations (100 mM) is within reach of existing HFIS platform designs.**

***Index Terms*—capacitive biosensor, high frequency impedance spectroscopy, nanoelectrodes, nanoelectronic biosensor array, numerical simulation, virus.**

I. INTRODUCTION

High frequency impedance spectroscopy (HFIS) has been used for the detection of a number of different analytes, such as microbeads [1], [2], [3], cells [1], [3], [4], [5], [6], [7], oil emulsions [3], gases [8], enzymes [9], DNA strands [10], and proteins [11]. Operation at high-frequency entails the possibility to overcome the screening induced on the electrolyte by the electrical double layer (EDL), and enables to extend the detection range beyond approximately one Debye length from the electrodes also in electrolytes at physiological salt concentration [12].

HFIS enables to detect analytes far from electrodes and to inspect different physical properties of analytes at different frequencies, such as charge dependence near the electrode's surface at low frequencies, or volume dependence at high frequency [13]. HFIS is enabled by nanoelectronic CMOS technology offering low parasitics, and very few implementation so far demonstrated operation above 1 MHz. The expected features of the capacitance response are thus largely unknown, and the effect of the electrolyte environment is also not so extensively explored.

In fact, examples of virus impedance/capacitance spectra recordings are given, for instance, in [14], [15] (for FIV, HIV, AV5, HSV1, SV40, MVA and CPMV viruses), showing that the viruses possess distinguishable capacitances and that dielectric properties of capsid proteins and glycoproteins (which are different for every viral type) significantly influence the observed response. However, these measurements do not rely on CMOS technology (thus losing the opportunities offered by technology scaling) and the maximum frequency of analysis is still below the electrolyte relaxation frequency at physiological salt concentrations.

[1] DPIA, University of Udine, via delle Scienze 206, 33100 Udine, Italy cossettini.andrea@spes.uniud.it

[2] Now with DIEF, University of Modena and Reggio Emilia, Modena, Italy

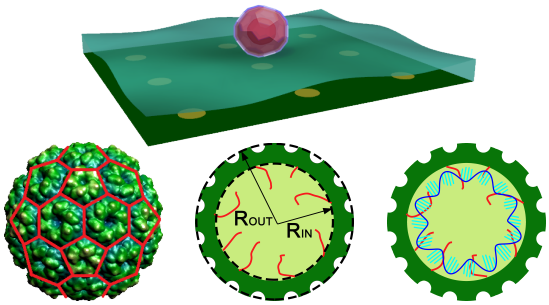

Fig. 1. *Top: sketch of the magnified truncated icosahedron model structure of the T=3 capsid attached to a BSA layer covering the electrodes (dimensions not in scale: $R_{electrodes} = 90$ nm, $R_{capsid} = [12-20]$ nm). Bottom left: representation of the T=3 CCMV virus, highlighting its truncated icosahedral symmetry (image taken from VIPERdb web portal [20]). Bottom center: 2D sketch of the capsid cross section. Red lines represent proteic tails which are not resolved by X-ray crystallography. The core of the virus is filled with electrolyte. Bottom right: same as bottom center graph with the RNA enclosed by the capsid [18].*

In this context, the present work reports impedance spectroscopy simulations up to high frequency to characterize the capacitance spectra of three T=3 viruses: a plant virus (the *Cowpea Chlorotic Mottle Virus*, CCMV), an animal virus (the *Rabbit Haemorrhagic Disease Virus*, RHDV), and a human virus (the *Hepatitis A Virus*, HAV). The structure and the morphology of isolated viruses is usually inspected by means of complex atomistic models [16], [17]. Rather than aiming at detailed and accurate virus descriptions, in this work we extend our previous report [18] and we use the atomistic data as the starting point to develop a compact and spatially averaged virus model, representative of the main geometrical and electrostatic properties and aimed at studying the HFIS response of a realistic CMOS nanoelectrode biosensor platform [19], by investigating the capacitance spectra properties of the three different viruses. The results reveal aspects of relevance for modeling and of practical importance to steer the design of successful experiments.

II. BIOSENSOR PLATFORM AND NUMERICAL MODELS

We consider the high frequency impedance spectroscopy CMOS biosensor platform presented in [19] and extensively described in [1], [3], as a reference test vehicle. The platform implements 256x256 individual nanoelectrodes with 90 nm radius and row/column pitches of 720 and 600 nm, respectively, and it is excited one row at a time repeatedly scanning the entire array approximately every 5 ms. The electrodes are alternatively charged and discharged at frequencies up to f=50 MHz via two n-MOS transistors actuated by non-overlapping clock signals. The switching capacitance at each electrode (C_{SW}) is computed from the measured integrated

This article has been accepted for publication in a future issue of this journal, but has not been fully edited. Content may change prior to final publication. Citation information: DOI 10.1109/TNB.2018.2826919, IEEE Transactions on NanoBioscience

charging current [21]. Analytes next to the electrodes perturb the electric field, generating detectable steps in the $\Delta C_{SW}(t)$ waveforms. More details on the platform are reported in [19], [1], [3].

Numerical simulations are performed generating tetrahedral meshes with *netgen* [22] and exploiting the in-house custom 3D CVFEM nanobiosensor simulator ENBIOS, which was extensively described in [23] and is also partly available via nanohub.org [24], [25]. ENBIOS solves self-consistently the Poisson-Boltzmann (PB) and Poisson drift-diffusion (otherwise denoted Poisson-Nernst-Planck, PNP) equations in DC and AC small signal regimes, respectively [26]. As in [18], the AC admittance of each electrode is computed from the simulated small signal current $\tilde{I}(\omega)$ divided by the applied voltage $\tilde{V}$: $Y(\omega)=\tilde{I}(\omega)/\tilde{V}=G(\omega)+j\omega C(\omega)$. We will present the capacitance spectra in terms of an *effective capacitance* $C_{eff}=|Y|/\omega$, which we verified to be an excellent approximation of the actual switching capacitance C_{SW} measured by the on chip detector [1].

III. VIRUSES AND MODELING METHODOLOGY

Viruses with T=3 triangulation number are defined by an icosahedral symmetry [27]. They are made up by a proteic capsid arranged in truncated icosahedral shape, and a nucleic acid is possibly enclosed within them.

Fig. 1 (bottom left) shows the icosahedral shape on top of a detailed atomistic contour map of a CCMV virus, and Fig. 1 (top) shows the generated capsid structure of T=3 viruses on top of the electrodes array. Part of the capsid proteins protrude into the inner core, generating proteic tails (Fig. 1, bottom center). The negatively charged nucleic acid interacts with the positive charge of the proteic tails, and it is thus located next to the capsid inner surface and with very low density at the center [16] (Fig. 1, bottom right).

The first virus we consider is the *Cowpea Chlorotic Mottle Virus* (CCMV). We select this virus as a plant virus example, and because it is common and well studied. CCMV is a ssRNA(+) virus with no external coating, made up only by the proteic capsid ($\approx$ 24 nm diameter) and a nucleic acid (RNA) within it [17], as also partly described in [18]. Its genome is composed of three distinct RNA molecules (RNA1, RNA2, RNA3) [28]. The longest sequence (RNA1) has 3174 nucleotides. The CCMV native form is stable for pH values between 3 and 6 and ionic strengths lower than 100 mM. Increasing the pH level results in an increase of the virus size (*swollen state*) [29], along with the formation of openings in the capsid's structure which allow the exchange of ions between the inner core of the virus and the outer electrolyte. On top of that, for large ionic strengths ($\approx$ 1 M) the complete disgregation of the capsid can also occur [17]. As in [18], we will first consider a pH of 5 and concentrations much smaller than 1 M, corresponding to the virus stable state, inspecting the capacitance spectra of empty capsids and full viruses (i.e., capsid + RNA). Electrolytes of different salt concentration will also be used. Then, we will also consider a higher pH value (7), taking into account the swelling process of the capsid [30].

As a second case study, we consider the *Rabbit Haemorrhagic Disease Virus* (RHDV) [31]. We select this virus as an animal virus example, and because of its economic and ecological importance [32]. As for the CCMV, it has a non-enveloped capsid (i.e., it has no external coating). On top of that, as reported in Sect. III-A6, it is also an interesting test case due to its mass distribution. The capsid of the RHDV is of about 27-40 nm in diameter, and its ssRNA(+) genome is 7.5 kb long. As for the CCMV, we investigate the capacitance spectra of the capsid and the full virus. Given its pH stability range ($4.5 < \text{pH} < 10.5$), we will consider physiological values of pH (7) and electrolyte salt concentration (NaCl 150 mM).

Finally, we analyze the *Hepatitis A virus* (HAV) [33], [34]. We select this non-enveloped virus as a human virus example. It is a nice test case because it is still an enigmatic virus, since it has proved to be quite difficult to study. Its ssRNA(+) genome is of about 7.48 kb long [34]. HAV remains stable up to 80 degrees and at pH levels down to 2. Thus, we will inspect its structure and capacitance spectra at different pH levels, for a physiological salt concentration electrolyte.

A. CAPSID MODEL

A continuum model suitable to analyze the virus–nanoelectrode interactions is desirable for the analysis of the electrical response. To this end, we extend the *double-shell* modeling approach of [35], in which the capsid is represented as a spherical shell with finite (non-zero) thickness. We build a truncated icosahedral shape, inscribed within two spheres of radii R_{IN} and R_{OUT}, as also sketched in Fig. 1 (bottom center). The methodology first presented in [18] has been refined in the present work. In order to build the capsid of the viruses:

1) ATOMS spatial position: the spatial position of the atoms (as obtained by X-ray crystallography) is taken from [20]. Hydrogen atoms and some mobile proteic tails not resolved by X-ray crystallography are not included in the list of atoms.

2) ATOMS missing H and fractional charge: we use the online tool *PDB2PQR* [36], which processes the list of atoms adding the missing hydrogen atoms and also correcting the charge values accounting for the pH-dependent atoms' fractional charge [37], [38].

3) AMINO ACIDS position: the position of each amino acid $\mathbf{R}_i$ is computed as the center of mass of the corresponding atoms: $\mathbf{R}_i = \sum_j m_{ij}\mathbf{r}_{ij}$, where m_{ij} and $\mathbf{r}_{ij}$ are the mass and the position of the j-th atom of the i-th amino acid, respectively. Due to their small mass, hydrogen atoms have a negligible

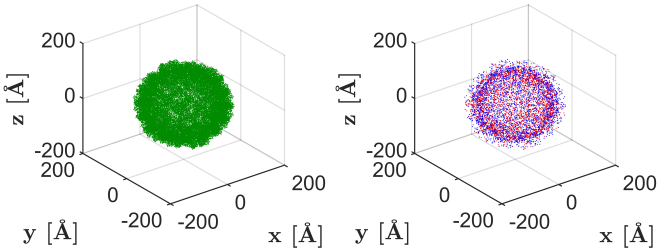

Fig. 2. *Left: 3D map representing the location of the amino acids of the capsid of the CCMV. Right: 3D map representing the charge (red: positive, blue: negative) corresponding to each amino acid of the CCMV.*

This article has been accepted for publication in a future issue of this journal, but has not been fully edited. Content may change prior to final publication. Citation information: DOI 10.1109/TNB.2018.2826919, IEEE Transactions on NanoBioscience

impact on the estimation of the position. As an example, Fig. 2 (left) shows a 3D map of the location of the atoms for the CCMV, as extracted with the described methodology.

4) AMINO ACIDS mass and charge: the mass of each amino acid (M_i, which is the sum of the masses of its atoms $M_i = \sum_j m_{ij}$) is computed according to [39] (hydrogen masses are included). A charge (Q_i) is assigned to the center of mass of each amino acid, and it is given by the sum of the fractional charges of the atoms belonging to the amino acid itself ($Q_i = \sum_j q_{ij}$, where q_{ij} is the charge of the j-th atom of the i-th amino acid, as shown in Fig. 2, right).

5) CAPSID mass and charge densities: the volume mass density and the volume charge density distributions are computed as a function of radial distance by averaging the local values over polar and azimuthal angles. Fig. 3 (top row) shows the averaged mass distributions for the three viruses under study. Fig. 3 (central row) shows the averaged charge distributions (at pH=5 for the CCMV, pH=7 for the RHDV, pH=7 for the HAV).

6) CAPSID dimension: Full Width Half Maximum (FWHM) limits of the mass distribution are extracted to identify R_{IN} and R_{OUT} (Fig. 3, top), following the approach of [35]. We verified that the bin width (2 Å) does not have major impact on the results, consistently with [35]. As anticipated, the mass distribution of the RHDV is peculiar, due to the presence of a density peak near the inner surface. As a consequence, the FWHM extraction does not properly represent the mass profile, since a large part of the right tail is excluded (Fig. 3, top center). To overcome this limitation, we extract Full Width Half Mean values instead. This approach entails a difference in the radii estimation of only 2 Å for the HAV, while it results in an increase of R_{OUT} by 1 nm for the CCMV. Table I reports the radial parameters for the different capsids under study.

7) CAPSID charges: the charges beyond the inner and outer surfaces of the capsid, Q_{IN} and Q_{OUT}, are computed summing the charges of the amino acids at distance $r < R_{IN}$ and $r > R_{OUT}$, respectively. As for the body of the capsid, i.e. $R_{IN} < r < R_{OUT}$, Ref. [40] concludes that the charges therein (Q_{BODY}) are essentially zero because the energy which is required to dissociate them is very high. Instead, Refs. [41], [42], [43] consider the amino acids in the body of the capsid as charged. As in [18], we will first discuss both cases for the CCMV; then, we will rely on the latter assumption for the other viruses.

8) CAPSID mobile tails: the charge of the unresolved amino acids of the mobile proteic tails is computed based on the database [44] and the online calculator [45], and it is added to Q_{IN}. Table I reports the final electrical parameters for the different capsids under study.

The above methodology was validated by generating the *cucumber mosaic virus* (CMV) model as a test case. The extracted model parameters are consistent with those reported in [35], thus proving the accuracy of the methodology. The truncated icosahedron model is inscribed into the spheres of radii R_{IN} and R_{OUT}. We assign Q_{IN} and Q_{OUT} as volume charges to δ=0.5 nm thick shells located at $[R_{IN} - \delta, R_{IN}]$ and $[R_{OUT} - \delta, R_{OUT}]$, respectively. We assign Q_{BODY}, when considered, to the remaining part of the capsid (i.e., in $[R_{IN}, R_{OUT} - \delta]$). As an example, Fig. 3 (bottom) reports the

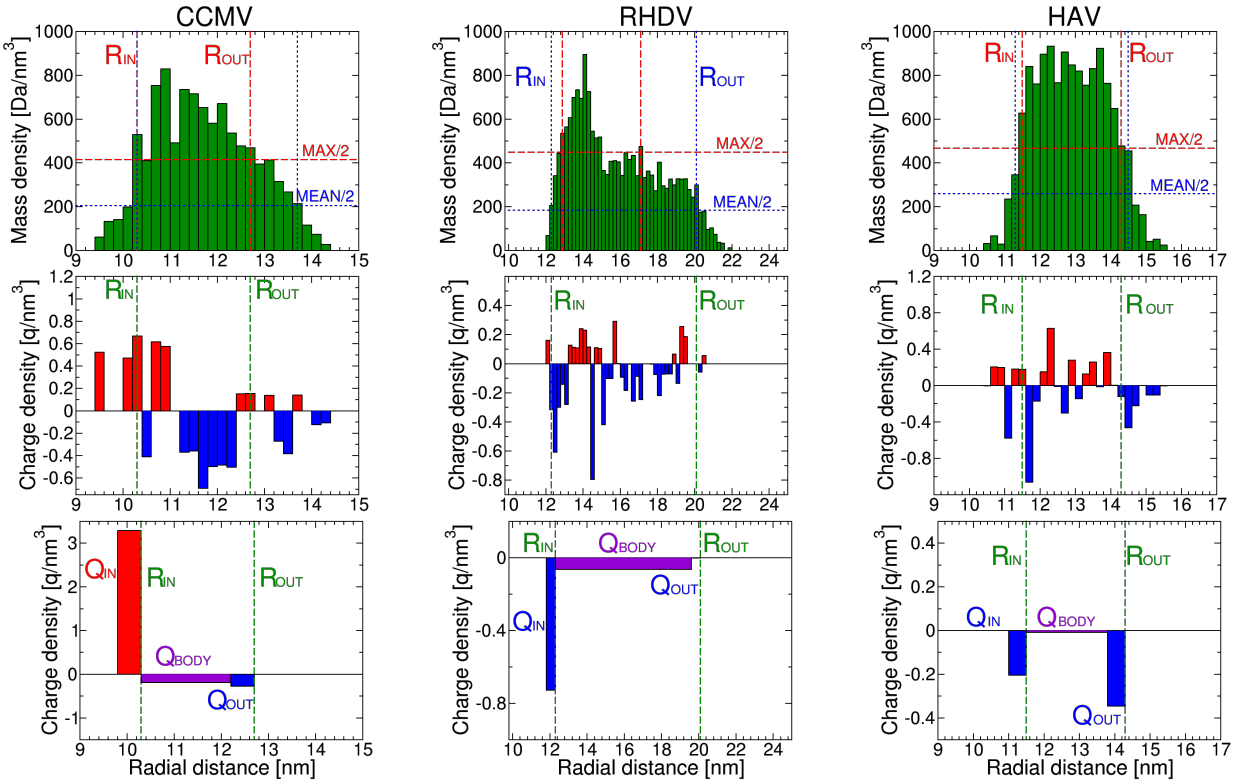

Fig. 3. *Geometrical and electrical models of the stable CCMV capsid (left column), RHDV capsid (center column), and HAV complete capsid (right column). Top row: density of mass radial distributions, highlighting R_{IN} and R_{OUT} and Full Width Half Max/Mean values. Central row: charge radial distributions, obtained at pH=5 for the CCMV, and pH=7 for the RHDV and the HAV. Bottom row: compact charge distributions assigned in the simulator.*

This article has been accepted for publication in a future issue of this journal, but has not been fully edited. Content may change prior to final publication. Citation information: DOI 10.1109/TNB.2018.2826919, IEEE Transactions on NanoBioscience

volume charge profiles (Q_{IN}, Q_{BODY}, and Q_{OUT}) as assigned for the numerical simulations of CCMV, RHDV and HAV capsids.

All the relevant geometrical and electrical parameters are summarized in Tab. I. Finally, the dielectric permittivity of the capsid body and shells ($r \in [R_{IN}-\delta, R_{OUT}]$) is set to ε_r=5, as in [46], whereas the core of the virus ($r \in [0, R_{IN}-\delta]$) is filled with electrolyte.

B. RNA MODEL

The nucleic acid possibly enclosed in the capsids contributes as well to the charge of the virus. We model the RNA as:
1) either an additional charge contributing to Q_{IN} (thus, with no change in volume of the shell at low dielectric constant),
2) or also partially filling the core of the CCMV (replacing the electrolyte with a low dielectric constant material in another 0.5 nm shell). Regarding the CCMV, it can be filled by three possible RNA sequences [28], and we show results for the longest one, which is 3174 nucleotides long. For the RHDV and the HAV, 7500 and 7480 nucleotides are considered, respectively [31], [34]. Since the RNA is partly immersed in electrolyte, we assign an effective charge of $-0.8q$ per nucleotide (instead of the theoretical $-1q$) to account for screening effects [18], as also reported in [46], [47].

The RNA carries a negative charge, that for the CCMV compensates the positive charge of the proteic tails. The full CCMV virus presents a negative Q_{IN} value, compared to the positive charge of the empty capsid (see Fig. 3 bottom left).

C. CAPSID WITH CHARGED BODY

As discussed in section III-A, the body of the capsid might not be completely neutral. To investigate this scenario, we take into account also the charge located in $R_{IN} < r < R_{OUT}$, and we set Q_{BODY} to this value [18].

The first and second columns of Table I report the model parameters for the CCMV following these two assumptions regarding the charge of the body. We will compare these two options for the CCMV case only (and, in this case only, for the sake of a worst case estimation a charge of $-1q$ per nucleotide is assumed for the "charged" capsid body), then relying on the "charged" model for RHSV and HAV viruses.

IV. NUMERICAL SIMULATIONS

The simulation setup follows the approach presented in [18]. An array of 5x5 electrodes is considered, and the AC excitation is applied to the central row of electrodes, mimicking the working principle of the biosensor platform [19]. A 3 nm thin dielectric BSA layer (24% water content) is included on the array surface as an analyte capture layer (Fig. 1 top) [48], [49]. We place the analyte at a distance of 0.5 nm from the BSA surface (unless otherwise stated). The typical mesh has $\approx$ 10k elements for the virus ($\approx$ 200k total) and the DC simulation runs in about 2.5 hours, with an approximately 2$\times$ increment if the virus body is discretized in three regions instead of just one. In the following we will inspect capacitance variation frequency spectra, i.e. $\Delta C_{eff} = C_{eff_{w/\ analyte}} - C_{eff_{w/o\ analyte}}$.

A. CCMV

Since it is practical to manipulate the CCMV with sodium acetate buffers [50], we first simulate the virus in a 100 mM $C_2H_3NaO_2$ electrolyte, and the capsid in 300 mM NaCl water electrolyte [18].

The left and right plots of Fig. 4 show the ΔC_{eff} spectra considering both the "neutral" and the "charged" model for the body of the capsid. We do also consider the cases in which the RNA is either an additional charge (with no inner electrolyte volume substitution), or it partially fills the core of the virus (thus replacing the electrolyte with a low permittivity region). ΔC_{eff} at 50 MHz (the operating frequency of the chip) is in the order of a few hundred zF. The difference between the capsid and virus responses is of the same order of magnitude [18]. As expected [13], the charge of the RNA in the CCMV has no impact on the high frequency response, affecting mainly the low frequency part of the curves. Q_{BODY} has a small impact on the capsid's spectrum, also due to the relatively high electrolyte salt concentration; conversely, it has a larger impact on the CCMV's, which is immersed in an electrolyte with lower salt concentration. The partial replacement of electrolyte with low dielectric constant RNA is visible mostly at low frequency; however, if Q_{BODY} is considered this impact is smaller (the response being mainly determined by the extra charge) [18].

Since different electrolyte salt concentrations shift the spectrum of ΔC_{eff} and amplify differences between the curves at 50 MHz, it would be of interest to compare the response of empty capsid and full CCMV in the same ambient conditions.

Parameter	**CCMV Capsid [18]** (neutral)	**CCMV Capsid [18]** (charged)	**CCMV Capsid Swollen 1** (charged)	**CCMV Capsid Swollen 2** (charged)	**RHDV Capsid** (charged)	**HAV Capsid** (charged)	**HAV Capsid Empty** (charged)
R_{IN}	10.3 nm	10.3 nm	12.7 nm	12.5 nm	*12.3 nm	11.5 nm	11.7 nm
R_{OUT}	12.7 nm	12.7 nm	15.5 nm	15.3 nm	*20.1 nm	14.3 nm	14.3 nm
Q_{IN}	+1812 q	+1812 q	+1962 q	+1842 q	-576 q	-141 q	238.8 q
Q_{BODY}	0	-550 q	-720 q	-660 q	-1320.6 q	-36.6 q	381 q
Q_{OUT}	-230 q	-230 q	-359 q	-300 q	-4.2 q	-372.6 q	-549.6 q

* Full Width Half Mean calculation

TABLE I

CCMV, RHDV and HAV capsids model parameters. The labels "neutral" and "charged" refer to the assumption of Ref. [40] and that of Refs. [41]–[43] for the charge in the body of the capsid, respectively. CCMV values correspond to pH=5. CCMV (swollen), RHDV, and HAV correspond to pH=7.

This article has been accepted for publication in a future issue of this journal, but has not been fully edited. Content may change prior to final publication. Citation information: DOI 10.1109/TNB.2018.2826919, IEEE Transactions on NanoBioscience

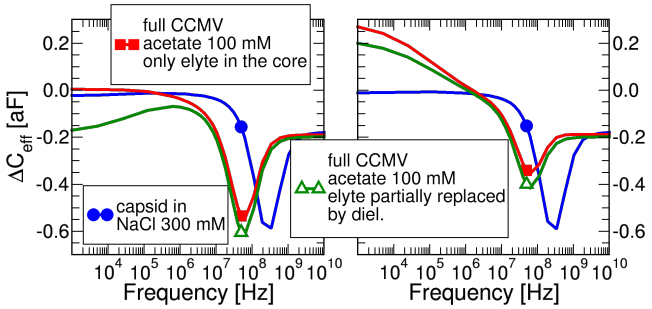

Fig. 4. *ENBIOS simulations of CCMV capsids in 300 mM NaCl water electrolyte and CCMV full viruses in 100 mM $C_2H_3NaO_2$ electrolyte. The symbols correspond to the 50 MHz point. The analyte is located 1 nm from the BSA surface. The capsid body is assumed without (left) and with (right) charge between R_{IN} and R_{OUT} [18].*

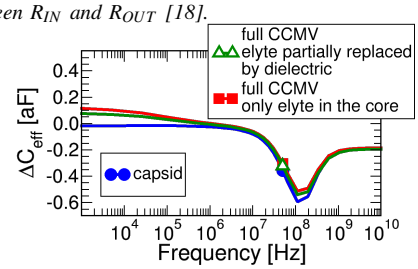

Fig. 5. *Same as Fig. 4 (right) with NaCl 150 mM electrolyte for all the curves, both for capsids and for full CCMVs [18].*

In Fig. 5, we make this comparison using a 150 mM NaCl electrolyte. The corresponding change of ΔC_{eff} between the empty capsid and full virus is reduced to only $\approx$ 50 zF at 50 MHz (unless the change of ε in the capsid core is considered): sensitivity should be improved to $\approx$ 10 zF to safely detect the difference [18].

These preliminary results suggest that while detection of one virus requires 0.1 aF sensitivity and resolution (a value demonstrated in [51] but only up to 1 MHz), discriminating the virus from the capsid requires approximately 10 zF sensitivity and resolution. Discrimination between the capsid and the infectious virus remains very challenging because the differences in response are mostly due to the electrolyte environment required by experiments.

At sufficiently high frequency, we can infer from Fig. 5 that the response to empty capsids is always larger (in absolute value) than the response to full CCMVs. However, the deposited BSA layer would inevitably be affected by surface roughness, and even more critically the biosensor coverage cannot be expected to be perfectly uniform over the whole array. For these reasons, the assumption that the response to empty capsids is always larger than the response to full CCMVs at 50 MHz may not always hold. To investigate this scenario, we run ENBIOS simulations of CCMV capsids and full viruses for different values of the BSA layer thickness. The results are shown in Fig. 6 (top), with the two insets highlighting how the capacitance variation changes with the BSA thickness at 1 kHz and at 50 MHz. The profile at 50 MHz (top-right inset), in particular, shows that less than 1 nm difference in BSA thickness can lead to a larger response for the CCMV. Fig. 6 (bottom) shows how the capacitance variation at low and high frequency changes according to the analyte vertical elevation above the BSA (d_z); due to the

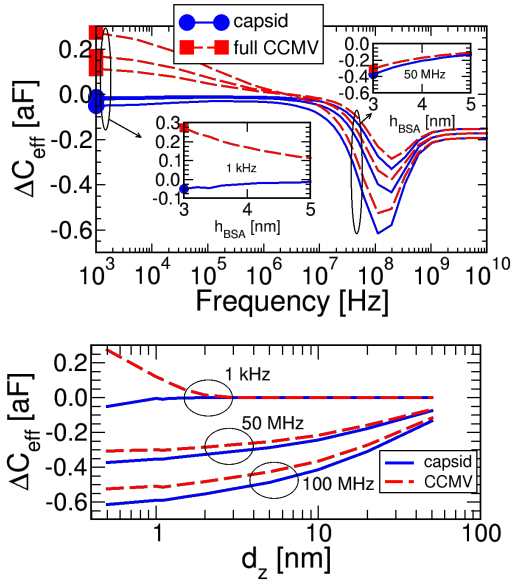

Fig. 6. *Families of ENBIOS simulations of CCMV capsid (blue curves) and full virus (red curves) for different BSA thickness values (h_{BSA}) or vertical elevation (d_z) above the BSA. For the full CCMV, the RNA is modeled as an additional charge (as for the red curve in Fig. 5). The electrolyte is NaCl 150 mM. Top: capacitance spectra for different h_{BSA} (3, 4, or 5 nm) with the analyte located at d_z = 0.5 nm. Bottom: capacitance variation response at three different frequencies as a function of d_z.*

screening induced by the EDL, the low frequency response essentially vanishes above a few Debye lengths, whereas at high frequency the discrimination is possible also at larger d_z.

As discussed at the beginning of Sect. III, an increase of the pH of the solution *swells* the capsid. In the following we investigate this scenario. A pathway for the pH-induced swelling process of the CCMV is described in [30], where the details of the loss of the interactions at the quasi-3-fold interfaces (occurring especially in the initial stages of the swelling process) are provided. The protein-protein interfaces vary during the swelling, and to characterize the progressive change of the structure the models of two intermediate states ("Swollen Form Model 1" and "Swollen Form Model 2") can be obtained from [20].

We analyze these models assuming pH=7. The third and fourth columns of Table I report the extracted values (radii and charges) for these two models. It must be noted that the differences with respect to the stable capsid arise not only due to different protein-protein interactions and amino acids spatial locations, but also due to the different pH of the environment. In particular, the charge of the unresolved amino acids of the mobile proteic tails (which is added to Q_{IN}) differs as well, as computed with [45].

Fig. 7 shows ENBIOS simulations for the stable capsid (at pH=5) and for the two intermediate swollen structures (at pH=7) in 150 mM NaCl electrolyte. At high frequency, the response is larger for the swollen capsids. A peak of 1 aF is obtained around 100 MHz, and the high frequency limit is at 0.33 aF (compared to the 0.2 aF for the stable CCMV). This behavior is explained mostly by the difference in volume, as also predicted by Eq. 10 and Fig. 5 in [13], since the charge plays a marginal role at very high frequencies. In fact, the response of the two swollen capsid models is essentially the same, since the volume difference is minimal. Differently, at

This article has been accepted for publication in a future issue of this journal, but has not been fully edited. Content may change prior to final publication. Citation information: DOI 10.1109/TNB.2018.2826919, IEEE Transactions on NanoBioscience

low frequency the response of the two swollen capsid models differ: due to the very close distance to the BSA surface, part of the capsid interacts with the electrical double layer. As a consequence, small variations in volume and charge can lead to larger variations of the capacitance profile.

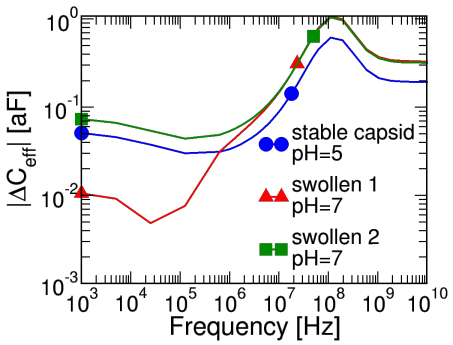

Fig. 7. *Comparison between ΔC_{eff} spectra of stable CCMV capsid and two models of swollen CCMV capsid. The analyte is located 0.5 nm from the BSA surface. The electrolyte is NaCl 150 mM.*

B. RHDV

As discussed in Sect. III-A6, we rely on a Full Width Half Mean estimation of the capsid size to avoid losing a significant part of the mass distribution, located beyond R_{OUT}. The RNA sequence enclosed by the capsid is approx. 7.5 kb long, corresponding to a partially screened charge of approximately -6000q [46], [47].

Fig. 8 compares the capacitance spectra of the empty capsid and the full virus, considering both approaches to extract the radii. As for the CCMV virus, the difference between empty capsids and full viruses is very small at high frequency, since it is mostly due to a difference in the charge profile and spectra at high frequency are weakly sensitive to charges. Regarding the two approaches for the radii estimation, as expected the Full Width Half Mean approach leads to larger capacitance variations (in absolute value), since the volume of the analyte is larger [13]. Due to the larger dimension, compared to the CCMV, a peak of about 2 aF can be noticed, whereas the high frequency limit leads to a capacitance variation of -0.8 aF.

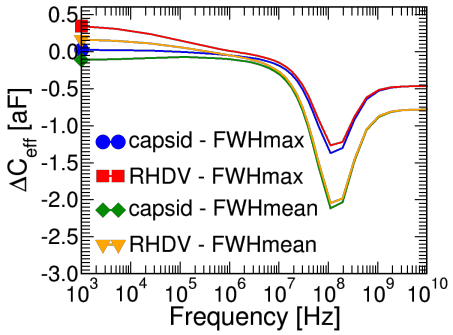

Fig. 8. *ΔC_{eff} spectra of RHDV capsid and full virus, considering the two models for the radii estimation. The analyte is located 0.5 nm from the BSA surface. The electrolyte is NaCl 150 mM.*

C. HAV

As anticipated in Sect. III, HAV remains stable down to pH=2. Hence, we investigate the charge distribution and the capacitance spectra at different pH levels.

Two models are available for the capsid of HAV [20]: the complete capsid and an "empty" capsid version (a number of amino acids is missing, compared to the complete model). As a first step, we compare the charge values (Q_{IN}, Q_{BODY}, Q_{OUT}) over different pH levels. Figure 9 (bottom) shows how the charges vary with the pH. For progressively lower pH values, the charge distribution within the capsid becomes more positive, as can also be noticed by inspecting the charge distributions at pH=3, pH=5, pH=7 (Fig. 9, top).

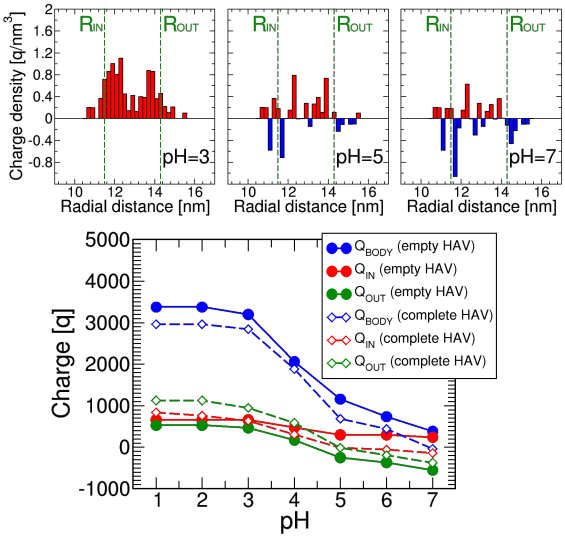

Fig. 9. *Top: HAV complete capsid charge distributions at pH=3, pH=5, pH=7. Bottom: HAV capsid charge values (Q_{IN}, Q_{BODY}, Q_{OUT}) as extracted with the described methodology at different pH levels. Two models for the HAV capsid are considered.*

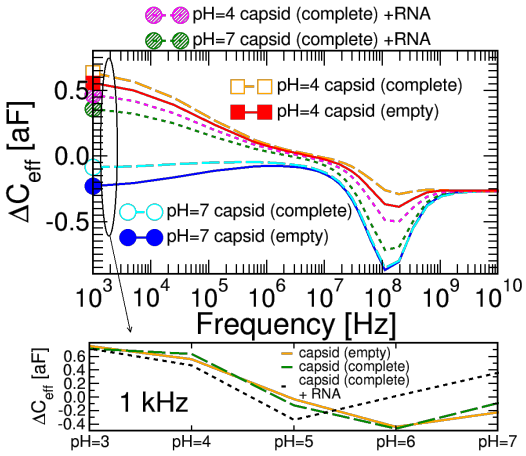

Fig. 10. *Top: ΔC_{eff} spectra of HAV capsid and full virus, considering the two models for the capsid. The analyte is located 0.5 nm from the BSA surface. The electrolyte is NaCl 150 mM. Bottom: low frequency capacitance variation for varying pH.*

In Fig. 10 we report capacitance spectra of complete and empty HAV capsids, at different pH levels. For the complete capsid, we do also show the spectra including the RNA charge. As expected, since the volume difference is minimal, the response to the two capsid models at high frequency is almost indistinguishable. At low frequency, due to the significant differences in volume charge, the two capsids can be easily discriminated. On top of that it must be noticed that the

This article has been accepted for publication in a future issue of this journal, but has not been fully edited. Content may change prior to final publication. Citation information: DOI 10.1109/TNB.2018.2826919, IEEE Transactions on NanoBioscience

response at different pH levels also changes remarkably, due to the different charge distributions (Fig. 9). This is in particular true at low frequency (Fig. 10 bottom)

V. DISCUSSION AND CONCLUSIONS

A methodology is proposed to study the response of a realistic HFIS platform to small viruses, and the case study of the CCMV, RHDV, and HAV viruses are discussed. Compact empirical models are derived for the viruses, which appear useful for the analysis of impedance sensing electronic devices. The methodology is quite general and can be adapted to the user's computational resources, possibly using finer lumping of the structure (e.g. sub-dividing the virus body in more slices), especially when high accuracy at low frequency is necessary.

The response at high-frequency is precisely proportional to the total volume Ω of the analyte including the electrolyte in the core [13], as shown in Fig. 11, regardless of the particle charge state. Deviation would be expected if the analyte were too close to the electrode [13], but this is not the case here since 3 nm of BSA is interposed between the array surface and the electrolyte. At low frequency, instead, there is no simple functional dependence to the volume. This is because the capacitance change is largely driven by the analyte charge. In fact, if we consider the low frequency limit of Fig. 7, we clearly see that the two swollen CCMV models, which have essentially the same volume but different charge values, yield different ΔC_{eff} values.

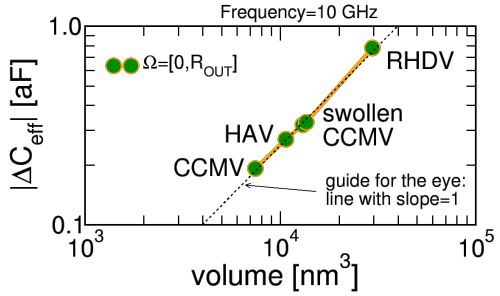

Fig. 11. *$|\Delta C_{eff}|$ at the high-frequency limit as a function of the total volume of the different T=3 viruses. The analytes are located 0.5 nm from the BSA surface. The electrolyte is NaCl 150 mM.*

The best detection conditions (maximizing $|\Delta C_{eff}|$) are found increasing the detection frequency above 100 MHz where ΔC_{eff} has a peak response. For the same electrolyte environment, the frequency of optimum sensitivity changes only slightly for the different viruses. This is consistent with the results reported in [13], in which the frequency corresponding to the peaks in the ΔC_{eff} spectrum is reported to depend only on the electrolyte salt concentration (via its relaxation frequency and Debye length) and the mean unperturbed electric field in the region occupied by the analyte. In fact, as it can be noticed from Figs. 5-8 and Fig. 10, top, the peak frequency is about 100 MHz in all the cases. This is because the electrolyte is always NaCl 150 mM, the analytes are all located in the same position and are small with respect to the electrode (hence, the difference in size between the different viruses does not significantly impact the value of the unperturbed electric field at the particle location). Moving to lower or higher salt concentration electrolytes (as in Fig. 4) clearly results in a decrease/increase of the peak frequency.

In summary, a number of qualitative and quantitative indications have been derived to identify the sensitivity and resolution requirements for optimal detection of small viruses and their charge state. Due to the fact that different portions of the capacitance spectra are sensitive to different factors (e.g., the charge affects the response especially at low frequency, the volume at high frequency), expanding the covered spectrum both at high frequency (facing the issue of parasitic capacitances) and low frequency (facing the issue of $1/f$ noise) would also be of interest. The proposed methodology is applicable to other viruses as well (provided the atoms' positions and partial charges are available) and it would thus be useful to build a library of HFIS spectra profiles for different virus families.

ACKNOWLEDGMENTS

We thank M. Dalla Longa, P. Scarbolo (University of Udine), F. P. Widdershoven (NXP Semiconductors), S. G. Lemay and C. Laborde (University of Twente) for fruitful discussions.

REFERENCES

[1] C. Laborde, F. Pittino, H. Verhoeven, S. Lemay, L. Selmi, M. Jongsma, and F. Widdershoven, "Real-time imaging of microparticles and living cells with CMOS nanocapacitor arrays," *Nature Nanotechnology*, vol. 10, no. 9, pp. 791–795, 2015.

[2] P. Scarbolo, E. Accastelli, T. Ernst, C. Guiducci, and L. Selmi, "Analysis of dielectric microbead detection by impedance spectroscopy with nanoribbons," in *Proc. IEEE NANO*, pp. 947–950, 2016.

[3] S. G. Lemay, C. Laborde, C. Renault, A. Cossettini, L. Selmi, and F. P. Widdershoven, "High-frequency nanocapacitor arrays: Concept, recent developments, and outlook," *Accounts of Chemical Research*, vol. 49, no. 10, p. 2355, 2016.

[4] R. W. Gajasinghe, O. Tigli, M. Jones, and T. Ince, "Label-free tumor cell detection and differentiation based on electrical impedance spectroscopy," in *Proc. IEEE SENSORS*, pp. 1–3, 2016.

[5] G. A. Cathcart, A. Tixier-Mita, S. Ihida, F. A. Shaik, and H. Toshiyoshi, "Transparent thin film transistor electrode array for real-time electrical impedance spectroscopy of cell cultures," in *Proc. IEEE NEMS*, pp. 379–383, 2016.

[6] V. Vijay *et al.*, "High-density CMOS microelectrode array system for impedance spectroscopy and imaging of biological cells," in *Proc. IEEE SENSORS*, pp. 1–3, 2016.

[7] H.-G. Jahnke *et al.*, "Impedance spectroscopy - an outstanding method for label-free and real-time discrimination between brain and tumor tissue in vivo," *Biosensors and Bioelectronics*, vol. 46, pp. 8–14, 2013.

[8] S. P. Basak, B. Kanjilal, P. Sarkar, and A. P. Turner, "Application of electrical impedance spectroscopy and amperometry in polyaniline modified ammonia gas sensor," *Synthetic Metals*, vol. 175, pp. 127–133, 2013.

[9] K.-S. Shin, J. H. Ji, K. S. Hwang, S. C. Jun, and J. Y. Kang, "Sensitivity enhancement of bead-based electrochemical impedance spectroscopy (beis) biosensor by electric field-focusing in microwells," *Biosensors and Bioelectronics*, vol. 85, pp. 16–24, 2016.

[10] S. W. Lee, T. Yamamoto, and T. Fujii, "Highly selective and sensitive DNA measurement by microelectrical impedance spectroscopy," in *Proc. TRANSDUCERS*, vol. 2, pp. 1314–1317, 2005.

[11] G. S. Kulkarni and Z. Zhong, "Detection beyond the Debye screening length in a high-frequency nanoelectronic biosensor," *Nano Letters*, vol. 12, no. 2, pp. 719–723, 2012.

[12] G. S. Kulkarni and Z. Zhong, "Fabrication of carbon nanotube high-frequency nanoelectronic biosensor for sensing in high ionic strength solutions," *Journal of Visualized Experiments: JoVE*, no. 77, 2013.

[13] F. Pittino, P. Scarbolo, F. Widdershoven, and L. Selmi, "Derivation and numerical verification of a compact analytical model for the AC admittance response of nanoelectrodes, suitable for the analysis and optimization of impedance biosensors," *IEEE Transactions on Nanotechnology*, vol. 14, no. 4, pp. 709–716, 2015.

[14] R. I. MacCuspie, N. Nuraje, S.-Y. Lee, A. Runge, and H. Matsui, "Comparison of electrical properties of viruses studied by ac capacitance scanning probe microscopy," *Journal of the American Chemical Society*, vol. 130, no. 3, pp. 887–891, 2008.
[15] M. Al Ahmad, F. Mustafa, L. M. Ali, J. V. Karakkat, and T. A. Rizvi, "Label-free capacitance-based identification of viruses," *Scientific reports*, vol. 5, 2015.
[16] D. Zhang, R. Konecny, N. A. Baker, and J. A. McCammon, "Electrostatic interaction between RNA and protein capsid in cowpea chlorotic mottle virus simulated by a coarse-grain RNA model and a Monte Carlo approach," *Biopolymers*, vol. 75, no. 4, pp. 325–337, 2004.
[17] J. A. Speir, S. Munshi, G. Wang, T. S. Baker, and J. E. Johnson, "Structures of the native and swollen forms of cowpea chlorotic mottle virus determined by X-ray crystallography and cryo-electron microscopy," *Structure*, vol. 3, no. 1, pp. 63–78, 1995.
[18] A. Cossettini, M. Dalla Longa, P. Scarbolo, and L. Selmi, "Modeling and simulation of small CCMV virus detection by means of high frequency impedance spectroscopy at nanoelectrodes," in *Proc. IEEE NANO*, pp. 416–419, 2017.
[19] F. Widdershoven *et al.*, "CMOS biosensor platform," *Proc. IEDM*, pp. 816–819, 2010.
[20] M. Carrillo-Tripp *et al.*, "VIPERdb2: an enhanced and web api enabled relational database for structural virology," *Nucleic Acids Research*, vol. 37, no. suppl 1, pp. D436–D442, 2009.
[21] J. Chen, B. McGaughy, D. Sylvester, and C. Hu, "An on-chip, attofarad interconnect charge-based capacitance measurement (CBCM) technique," in *Proc. IEDM*, pp. 69–72, 1996.
[22] J. Schöberl, "NETGEN an advancing front 2D/3D-mesh generator based on abstract rules," *Computing and Visualization in Science*, vol. 1, pp. 41–52, 1997.
[23] F. Pittino and L. Selmi, "Use and comparative assessment of the CVFEM method for Poisson-Boltzmann and Poisson-Nernst-Planck three dimensional simulations of impedimetric nano-biosensors operated in the DC and AC small signal regimes," *Computational Methods in Applied Mechanics and Engineering*, pp. 902–923, 2014.
[24] P. Scarbolo, F. Pittino, M. Dalla Longa, A. Cossettini, and L. Selmi, "ENBIOS-1D Lab, v3.0," Apr 2017. [Online]. Available: https://nanohub.org/resources/biolab, doi: 10.4231/D3GX44W13.
[25] A. Hoxha, P. Scarbolo, A. Cossettini, F. Pittino, and L. Selmi, "ENBIOS-2D Lab, v1.0," Oct 2016. [Online]. Available: https://nanohub.org/resources/biolabisfet, doi: 10.4231/D3V11VM7D.
[26] C. Heitzinger, Y. Liu, N. J. Mauser, C. Ringhofer, and R. W. Dutton, "Calculation of fluctuations in boundary layers of nanowire field-effect biosensors," *Journal of Computational and Theoretical Nanoscience*, vol. 7, no. 12, 2010.
[27] D. L. Caspar and A. Klug, "Physical principles in the construction of regular viruses," in *Cold Spring Harbor symposia on quantitative biology*, vol. 27, pp. 1–24, Cold Spring Harbor Laboratory Press, 1962.
[28] R. Francki, "The viruses and their taxonomy," in *The Plant Viruses*, pp. 1–18, Springer, 1985.
[29] R. Konecny *et al.*, "Electrostatic properties of cowpea chlorotic mottle virus and cucumber mosaic virus capsids," *Biopolymers*, vol. 82, no. 2, pp. 106–120, 2006.
[30] F. Tama and C. L. Brooks, "The mechanism and pathway of ph induced swelling in cowpea chlorotic mottle virus," *Journal of molecular biology*, vol. 318, no. 3, pp. 733–747, 2002.
[31] D. Luque *et al.*, "Epitope insertion at the n-terminal molecular switch of the rabbit hemorrhagic disease virus T=3 capsid protein leads to larger T= 4 capsids," *Journal of virology*, vol. 86, no. 12, pp. 6470–6480, 2012.
[32] E. Angulo and J. Bárcena, "Towards a unique and transmissible vaccine against myxomatosis and rabbit haemorrhagic disease for rabbit populations," *Wildlife Research*, vol. 34, no. 7, pp. 567–577, 2008.
[33] X. Wang *et al.*, "Hepatitis A virus and the origins of picornaviruses," *Nature*, vol. 517, no. 7532, pp. 85–88, 2015.
[34] J. L. Melnick, "Properties and classification of hepatitis a virus," *Vaccine*, vol. 10, pp. S24–S26, 1992.
[35] A. L. Božič, A. Šiber, and R. Podgornik, "How simple can a model of an empty viral capsid be? Charge distributions in viral capsids," *Journal of Biological Physics*, vol. 38, no. 4, pp. 657–671, 2012.
[36] T. J. Dolinsky, J. E. Nielsen, J. A. McCammon, and N. A. Baker, "PDB2PQR: an automated pipeline for the setup of poisson–boltzmann electrostatics calculations," *Nucleic Acids Research*, vol. 32, no. suppl 2, pp. W665–W667, 2004.
[37] C. R. Søndergaard, M. H. Olsson, M. Rostkowski, and J. H. Jensen, "Improved treatment of ligands and coupling effects in empirical calculation and rationalization of pk_a values," *Journal of Chemical Theory and Computation*, vol. 7, no. 7, pp. 2284–2295, 2011.
[38] M. H. Olsson, C. R. Søndergaard, M. Rostkowski, and J. H. Jensen, "PROPKA3: consistent treatment of internal and surface residues in empirical pk_a predictions," *Journal of Chemical Theory and Computation*, vol. 7, no. 2, pp. 525–537, 2011.
[39] E. Antezana, "The amino acid masses." [Online]. Available: http://education.expasy.org/student_projects/isotopident/htdocs/aa-list.html. [Accessed: Mar 2017].
[40] A. V. Finkelstein and O. B. Ptitsyn, *Protein Physics*. 2002.
[41] M. R. Gunner, J. Mao, Y. Song, and J. Kim, "Factors influencing the energetics of electron and proton transfers in proteins. what can be learned from calculations," *Biochimica et Biophysica Acta (BBA)-Bioenergetics*, vol. 1757, no. 8, pp. 942–968, 2006.
[42] D. G. Isom, B. R. Cannon, C. A. Castañeda, A. Robinson, and B. Garcia-Moreno E, "High tolerance for ionizable residues in the hydrophobic interior of proteins," *Proceedings of the National Academy of Sciences of the United States of America*, vol. 105, no. 46, pp. 17784–17788, 2008.
[43] D. G. Isom, C. A. Castañeda, B. R. Cannon, P. D. Velu, and B. Garcia-Moreno E, "Charges in the hydrophobic interior of proteins," *Proceedings of the National Academy of Sciences of the United States of America*, vol. 107, no. 37, pp. 16096–16100, 2010.
[44] UniProt Consortium *et al.*, "Ongoing and future developments at the universal protein resource," *Nucleic Acids Research*, vol. 39, no. suppl 1, pp. D214–D219, 2011.
[45] C. Putnam, "Protein calculator v3.4," 2016. [Online]. Available: http://protcalc.sourceforge.net/. [Accessed: Mar 2017].
[46] A. Siber, A. L. Bozic, and R. Podgornik, "Energies and pressures in viruses: contribution of nonspecific electrostatic interactions," *Physical Chemistry Chemical Physics*, vol. 14, pp. 3746–3765, 2012.
[47] M. Aubouy, E. Trizac, and L. Bocquet, "Effective charge versus bare charge: an analytical estimate for colloids in the infinite dilution limit," *Journal of Physics A: Mathematical and Theoretical*, vol. 36, no. 22, p. 5835, 2003.
[48] J. Eden, P. R. Gascoyne, and R. Pethig, "Dielectric and electrical properties of hydrated bovine serum albumin," *Journal of the Chemical Society, Faraday Transactions 1: Physical Chemistry in Condensed Phases*, vol. 76, pp. 426–434, 1980.
[49] D. Kim and A. E. Herr, "Protein immobilization techniques for microfluidic assays," *Biomicrofluidics*, vol. 7, no. 4, p. 041501, 2013 and references therein.
[50] D. Luque *et al.*, "Self-assembly and characterization of small and monodisperse dye nanospheres in a protein cage," *Chemical Science*, vol. 5, no. 2, pp. 575–581, 2014.
[51] M. Carminati, G. Ferrari, F. Guagliardo, and M. Sampietro, "Zeptofarad capacitance detection with a miniaturized CMOS current front-end for nanoscale sensors," *Sensors and Actuators A: Physical*, vol. 172, no. 1, pp. 117–123, 2011.

Andrea Cossettini (S'15) received the M.Sc. degree in Electronic Engineering from the University of Udine, Italy, in 2015. In 2014, he was at Acreo Swedish ICT AB (Kista, Sweden), designing waveguide-to-chip transitions at sub-mm waves. In 2015, he was at Infineon Technologies (Villach, Austria), working on signal integrity for high-speed serial interfaces. He is currently pursuing his Ph.D. working on electronic nano-biosensors. His current research interests include simulation, modeling, and characterization of electronic nano-biosensors.

Luca Selmi (M'01–SM'09–F'15) received the Ph.D. degree in Electronic Engineering from the University of Bologna, Italy, in 1992. Since 2000, he is Professor of Electronics. He served as TPC member of various conferences, including IEEE IEDM, IEEE VLSI Tech. Symposium, and as Editor of IEEE EDL. His research interests include simulation, modeling, and characterization of nanoscale CMOS transistors, with a recent twist toward nanoelectronic (bio)sensors.